First-principles study of Zr–N crystalline phases: phase stability, electronic and mechanical properties†

Shuyin Yu,*[ab] Qingfeng Zeng,[ab] Artem R. Oganov,[bcde] Gilles Frapper,[f] Bowen Huang,[f] Haiyang Niu[c] and Litong Zhang[a]

Using a variable-composition *ab initio* evolutionary algorithm, we investigate stability of various Zr–N compounds. Besides the known ZrN and Zr_3N_4, new candidate structures with Zr : N ratios of 2 : 1, 4 : 3, 6 : 5, 8 : 7, 15 : 16, 7 : 8 and 4 : 5 are found to be ground-state configurations, while Zr_3N_2 has a very slightly higher energy. Besides Zr_2N, the newly discovered Zr_xN_y compounds adopt rocksalt structures with ordered nitrogen or zirconium vacancies. The electronic and mechanical properties of the zirconium nitrides are further studied in order to understand their composition–structure–property relationships. Our results show that bulk and shear moduli monotonically increase with decreasing vacancy content. The mechanical enhancement can be attributed to the occurrence of more Zr–N covalent bonds and weakening of the ductile Zr–Zr metallic bonds. These simulations could provide additional insight into the vacancy-ordered rocksalt phases that are not readily apparent from experiments.

1 Introduction

Group IVB transition metal (TM = Ti, Zr and Hf) nitrides have been widely used in cutting tools and as wear-resistant coatings, because of their excellent properties such as high hardness and strength, high melting points, excellent thermal conductivity, and good chemical stability.[1–4] Formally, their mononitrides adopt the rocksalt structure, but may show significant variation in composition, both towards cation and anion enrichment.[1] Such nonstoichiometry widely exists in group IV/V transition metal oxides, nitrides and carbides, due to the formation of structural vacancies.[5] The concentration of vacancies can be up to 50 at%. Their microstructures are usually controlled by the co-precipitation of nonstoichiometric phases, and the mechanical behavior is dependent on the vacancy concentration.

[a]*Science and Technology on Thermostructural Composite Materials Laboratory, Northwestern Polytechnical University, Xi'an, Shaanxi 710072, China. E-mail: yushuyin2014@gmail.com*

[b]*International Center for Materials Discovery, Northwestern Polytechnical University, Xi'an, Shaanxi 710072, China*

[c]*Department of Geosciences, Center for Materials by Design, Institute for Advanced Computational Science, State University of New York, Stony Brook, NY 11794-2100, USA*

[d]*Skolkovo Institute of Science and Technology, 3 Nobel Street, Skolkovo 143025, Russia*

[e]*Moscow Institute of Physics and Technology, Dolgoprudny, Moscow Region 141700, Russia*

[f]*IC2MP UMR 7285, Université de Poitiers, CNRS, 4, rue Michel Brunet, TSA 51106, 86073 Poitiers Cedex 9, France*

† Electronic supplementary information (ESI) available. See DOI: 10.1039/c6ra27233a

Unlike carbides, not only nonmetal vacancies exist, but structure can also tolerate metal atom vacancies since metal atom oxidation state can reach +4.[6] Experimental investigations of nonstoichiometric TM nitrides (TM = Ti, Zr, Hf, V, Nb and Ta) have been conducted intensely for more than thirty years.[7–10] About twenty ordered carbides and nitrides have been found.[1] However, it has not yet been possible to construct a single phase diagram of TM–C or TM–N systems at low temperatures (most of the available phase diagrams have been constructed above 1300–1500 K). In this paper, we explore stable compounds in the Zr–N system at ambient pressure and finite temperatures. To date, there is no comprehensive and inclusive computational investigation of phase stability in the Zr–N system.

Zirconium nitrides represent a rich family of phases where the stability and microstructures are still not completely understood. According to the phase diagram provided by Gribaudo *et al.*,[11] ZrN and Zr_3N_4 can be stable at ambient conditions. In 2003, c-Zr_3N_4 with a Th_3P_4 structure was synthesized by Zerr *et al.* using diamond-anvil cell experiments at 16 GPa and 2500 K.[12] This compound was expected to exhibit a very high Vickers hardness around 30 GPa, similar to that of γ-Si_3N_4. However, Kroll showed that hardness is just slightly harder than 14 GPa.[13] Besides c-Zr_3N_4, an orthorhombic *Pnma* modification of Zr_3N_4 has been proposed.[14] First-principles calculations show that o-Zr_3N_4 is energetically more stable than c-Zr_3N_4.[15] However, both structures are metastable considering decomposition into ZrN and N_2.[13] Besides, two nitrogen-rich phases ZrN_x (1.06 < x < 1.23) with NaCl-type structures have been claimed by Juza *et al.* in 1964.[16] However, precise stoichiometries and crystal structures are not known for their synthesized samples.

Here, we apply recently developed evolutionary algorithm USPEX to extensively explore the crystal structures and stoichiometries in the Zr–N system at ambient conditions, and then their phase stability at finite temperatures are evaluated. Furthermore, the electronic and mechanical properties of stable Zr_xN_y compounds are studied using density functional theory. Our work should provide guidance for experimental groups aiming to synthesize these new technologically useful materials.

2 Computational details

Searches for low-energy crystalline Zr–N structures were performed using evolutionary algorithm (EA) methodology implemented in the USPEX code[17–19] in its variable-composition mode.[20] The energies and structural optimizations (including lattice shape, volume and atomic positions) were calculated by VASP package based on density-functional theory.[21] The first generation contained 80 randomly produced candidate structures, which were produced under the following constraints: (1) all possible stoichiometries were allowed, (2) the maximum number of atoms is 30 in the primitive cell. In the subsequent generations, each generation contained 60 structures, which were produced by applying heredity (50%), atom transmutation (20%), lattice mutation (15%) operators, while some structures were still randomly (15%). These are typical parameters for USPEX calculations, with which efficiency is known to be very high. Besides, we also performed a fixed-composition search for $Zr_{15}N_{16}$ which has 31 atoms in its primitive cell.

First-principles electronic structure calculations were carried out within the generalized gradient approximation (GGA) in the Perdew–Burke–Ernzerhof form.[22] The interactions between ions and electrons were described by the projector-augmented wave method[23] with a cutoff energy of 600 eV. Uniform Γ-centered k-points meshes with a resolution of $2\pi \times 0.03$ Å^{-1} and Methfessel–Paxton electronic smearing[24] were adopted for the integration in the Brillouin zone. These settings ensure convergence of the total energies to within 1 meV per atom. Structure relaxation proceeded until all forces on atoms were less than 1 meV Å^{-1} and the total stress tensor was within 0.01 GPa of the target value.

Theoretical phonon spectra were calculated with the supercell method using the PHONOPY package.[25] Hellmann–Feynman forces exerted on all atoms in supercells ($2 \times 2 \times 2$ of the unit cell) were calculated by finite atomic displacements of each symmetrically nonequivalent atom. Phonon dispersion relations were then obtained by the diagonalization of the dynamical matrix. We used the quasiharmonic approximation to calculate the free energy of zirconium nitrides at finite temperatures. Free energy of a crystal was obtained as a sum of the static total energy, vibrational energy and configurational energy. Computational details are described in ESI.†

3 Results and discussion

3.1 Phase stability of the Zr–N system at finite temperatures

Thermodynamic stability of zirconium nitrides in the temperature range of 0–2000 K was quantified by constructing the thermodynamic convex hull, which is defined as the Gibbs free energy of formation of the most stable phases at each composition:

$$\Delta G(Zr_xN_y) = [G(Zr_xN_y) - xG(Zr) - yG(N)]/(x + y) \quad (1)$$

Any phase located on the convex hull is considered to be thermodynamically stable (at $T = 0$ K, $G = H$) and at least in principle synthesizable.[26] In the case of zirconium nitrides, a series of stable compounds at various Zr : N ratios, *i.e.* 2 : 1, 4 : 3, 6 : 5, 8 : 7, 1 : 1, 15 : 16, 7 : 8, 4 : 5 have been discovered by our evolutionary searches at 0 K, shown in Fig. 1. The rocksalt ZrN with space group (SG) $Fm\bar{3}m$ was found to have the lowest enthalpy of formation. Besides ZrN, substoichiometric Zr_2N (SG: $P4_2/mnm$), Zr_4N_3 (SG: $C2/m$), Zr_6N_5 (SG: $C2/m$) and Zr_8N_7 (SG: $C2/m$) have also been found to be thermodynamically stable. For the missing composition Zr_3N_2, the lowest-energy structure is $Immm$ with the enthalpy of formation lying very close to the convex hull at only 0.005 eV per atom, *i.e.* Zr_3N_2 is a metastable phase at 0 K.

Additionally, Juza *et al.* in 1964 have discovered two nitrogen-rich phases ZrN_x ($1.06 < x < 1.23$) with rocksalt structures.[16] The synthesized sample had a dark blue color and turned into metallic ZrN upon heating. Unfortunately, detailed stoichiometries and crystallographic information were not determined. Subsequent studies even questioned the existence of these two compounds.[11] From our evolutionary searches, we found these two compounds could be $Zr_{15}N_{16}$ ($x = 1.07$, SG: $P\bar{1}$) and Zr_4N_5 ($x = 1.25$, SG: $C2/m$). Their structures are composed of edge-sharing ZrN_6 and $\square N_6$ ($\square$ means Zr vacancy) octahedra, similar to the rocksalt ZrN structure. To the best of our knowledge, such nitrogen-rich nitrides have never been reported in other TM–N systems. For Zr_3N_4, the most stable structure has the orthorhombic $Pnma$ symmetry,[27] which is
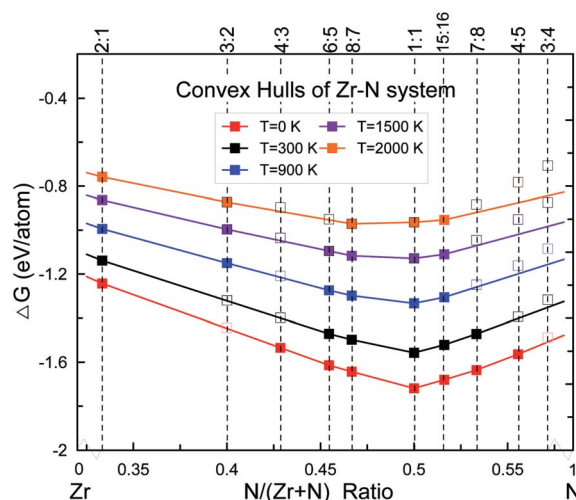

Fig. 1 Convex hulls of the Zr–N system in the temperature range of 0–2000 K at ambient pressure. The solid squares represent stable structures, while open ones denote metastable structures. The solid $P6_3/mmc$ phase of Zr, α-N_2 ($T = 0$ K) and N_2 gas ($T \geq 300$ K) were adopted as reference states.

energetically more favorable than the Th_3P_4-type structure by $\sim$0.019 eV per atom at 0 GPa and 0 K. We found it is thermodynamic metastable considering decomposition into ZrN and N_2 at ambient conditions. First-principles calculation shows that o-Zr_3N_4 will transform into c-Zr_3N_4 at $\sim$2 GPa (Fig. S2†).

We have carefully calculated the temperature contribution to the phase stability of the new discovered zirconium nitrides from 0 K to 2000 K within the quasiharmonic approximation, as shown in Fig. 1. Note that for each stoichiometry, the space group/structure found at 0 K is kept for higher temperatures. The free energies of formation increase with increasing temperatures for all phases but at different rates, yielding a convex hull which changes with temperature. Our results show that Zr_2N, Zr_8N_7, ZrN and $Zr_{15}N_{16}$ will not lose their stability in the whole studied temperature range. The unstable Zr_3N_2 at 0 K will become stable at temperatures higher than $\sim$900 K, while for Zr_4N_3, Zr_6N_5, Zr_7N_8 and Zr_4N_5, the temperature contributions have negative effect on their structural stability. For example, the formation enthalpy of reaction $2Zr_4N_5 (s) \rightarrow 8ZrN (s) + N_2 (g)$ will become negative above 300 K, which means Zr_4N_5 should decompose into ZrN and N_2 gas at roughly room temperature if associated kinetic barrier allows this process, perfectly consistent with the results of Juza et al.[16]

Crystal structures of the representative zirconium-rich Zr_6N_5 and nitrogen-rich Zr_4N_5 are schematically shown in Fig. 2, while other structures and their corresponding phonon dispersion curves are shown in Fig. S3 and S4.† No imaginary phonon frequencies are found, indicating their dynamical stability. The detailed crystallographic data, enthalpies and zero-point energies are listed in Table S1.† From Table S1,† we can find the computed lattice parameters for ZrN and Zr_3N_4 are in good agreement with those obtained from other theoretical and experimental investigations, which confirms the accuracy of our calculations. From the structural point of view, ZrN has the ideal cubic rocksalt structure, while $Zr_{n+1}N_n$ ($n = 2, 3, 5, 7$) and Zr_mN_{m+1} ($m = 4, 7, 15$) are versions of the rocksalt structure with ordered nitrogen or zirconium vacancies (Zr_2N has rutile-type structure).

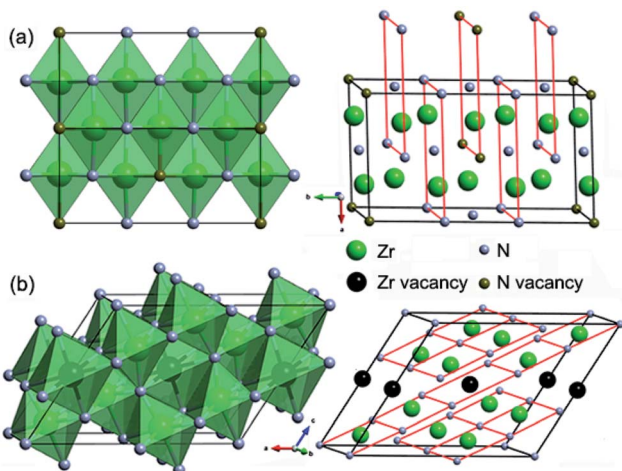In the structures of Zr-rich phases, the metal atoms form hexagonal close-packed (hcp) sublattices with N atoms filled in the octahedral voids, thus each N atom is coordinated by six Zr atoms, forming NZr_6 octahedra. However, the concentration of filled octahedral voids in various $Zr_{n+1}N_n$ structures is different. Two thirds of them are filled in Zr_3N_2; while seven eighths in Zr_8N_7. Similar nitrogen vacancy-ordered structures were also reported earlier to be stable for transition metal carbides $M_{n+1}C_n$ (M = Hf and $n = 2, 5$;[28] M = Zr and $n = 1, 2, 3, 6$;[29] M = Ti and $n = 1, 2, 5$ (ref. 30)) and nitrides $M_{n+1}N_n$ (M = Ti and $n = 1, 2, 3, 5$ (ref. 31)). For N-rich phases, one eighth of the metal atoms are replaced with vacancies in Zr_7N_8, while one fifth in Zr_4N_5.

The formation of such N-rich phases could be attributed to the enhanced stability of the +4 oxidation state of Zr and Hf compared to Ti due to the relativistic effects,[32] leading to the coexistence of +3 in MN and +4 in M_3N_4, while in the Ti–N system, TiN has the highest nitrogen content under normal conditions. In the structures of Zr_3N_4, the hcp metal framework of the rocksalt structure is significantly distorted. For o-Zr_3N_4, there are three nonequivalent types of Zr atoms, one of them is octahedrally coordinated to six N atoms, one resides at the center of a trigonal prism, and the last one is located inside of a heavily distorted octahedron (Fig. S3†). Thus, the second and third nonequivalent Zr atoms are sevenfold coordinated, while in c-Zr_3N_4, each Zr atom is coordinated to eight N atoms.

3.2 Electronic properties and chemical bonding

We calculated the electronic properties (density of states, DOS, see Fig. 3) of zirconium nitrides at ambient conditions in order to study their chemical bonding. Let us start first with Zr_3N_4 and then discuss the effect of zirconium or nitrogen vacancies on the electronic properties of rocksalt based-structures. In DOS of

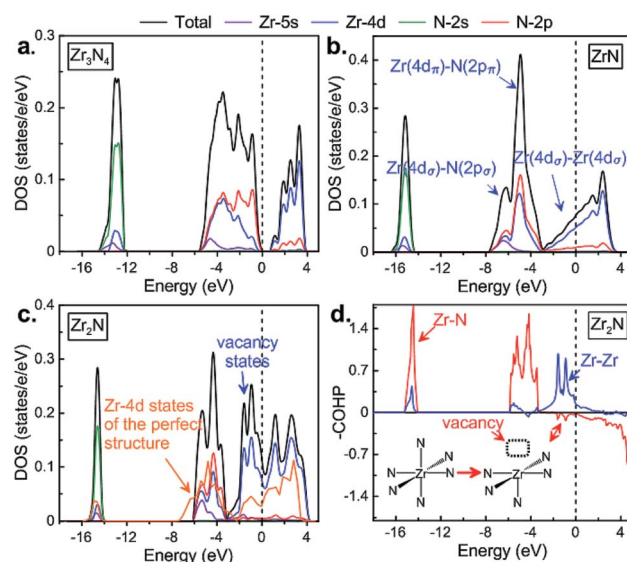**Fig. 2** Crystal structures of the representative (a) Zr_6N_5 and (b) Zr_4N_5 compounds.

Fig. 3 The calculated electronic density of states of (a) o-Zr_3N_4, (b) ZrN and (c) Zr_2N. (d) Crystal orbital Hamilton population ($-$COHP) curves of Zr_2N.

o-Zr_3N_4 displayed in Fig. 3a, three main regions may be described with three kinds of molecular orbital overlaps: nonbonding, bonding and antibonding.[33] Firstly, a rather sharp peak at roughly −13 eV appears and it is mainly of N(2s) character although with some Zr(4d) character. This sharp peak reflects the localized character of the nonbonding N(2s)-based levels; secondly, from −6 eV to 4 eV, a very broad structure with two well-defined main peaks originates from mixing of Zr(4d) and N(2p) orbitals. The lower peak corresponds to the bonding states, and the antibonding counterparts appear just above the Fermi level. These bonding and antibonding peaks exhibit a clear mixing of metal 4d and nitrogen 2p states, although the latter has a stronger Zr(4d) character. In o-Zr_3N_4, the gap separates bonding and antibonding states, thus Zr_3N_4 is a semiconductor and possesses a remarkable stability. Its calculated band gap (0.68 eV) is consistent with previous theoretical results.[6,13] These findings are understandable if one considers the following Zintl picture: Zr is in a formal oxidation state of +4 (Zr^{4+}, d^0), and N^{3-} follows the octet rule.

For the well-known stoichiometric rocksalt Zr_xN_y, we will first briefly discuss their electronic properties, then analyze the electronic perturbation due to the creation of nitrogen or zirconium vacancies – empty octahedral sites in the fcc network – leading to symmetry-broken $Zr_{n+1}N_n$ and Zr_mN_{m+1} structures. Similarly to o-Zr_3N_4, DOS of Zr_xN_y phases can be decomposed into three well-separated energy regions as shown in Fig. 3 and S5,† but here no gap separates the valence and conducting bands: (1) a deep lowest valence band, s_N; (2) hybridized Zr(4d)/N(2p) band, d_Mp_N; (3) a partially filled higher-energy Zr(4d) band, d_M. The s_N band is dominated by the 2s orbitals of the nitrogen atoms and is nonbonding. The next group of valence bands, d_Mp_N, results from strong hybridization of the 4d states of zirconium atoms with 2p states of nitrogen atoms. Also, one may see that for Zr_xN_y the bottom of the d_M band, dominated by 4d orbitals of zirconium atoms, responsible for metallicity.

When nitrogen vacancies are created in substoichiometric $Zr_{n+1}N_n$ ($n = 1, 2, 3, 5$ and 7), notice that obviously the formal oxidation state of Zr decreases as the number of nitrogen vacancies increases, going from Zr^{3+} d^1 in ZrN to $Zr^{1.5+}$ $d^{2.5}$ in Zr_2N. Therefore, one may expect the occupation of the Zr 4d levels in substoichiometric $Zr_{n+1}N_n$ compounds. This is what happens: Zr–Zr bonding and nonbonding (slightly antibonding) Zr–N levels appear just below the Fermi level, mainly metal 4d in character (see Fig. 3d and S6†). In $Zr_{n+1}N_n$, Zr atoms are no longer all in the MN_6 octahedral environment; some of them are in MN_5 square pyramidal configurations. Therefore, one may expect the stabilization of antibonding Zr–N levels when going from formally octahedral ZrN_6 to square pyramidal ZrN_5 environment due to the lack of a Zr(4d)–N(2p) antibonding component. The occupation of these Zr–N nonbonding levels may explain the mechanical properties of these substoichiometric $Zr_{n+1}N_n$ compounds.

Fig. 3c displays the total and projected DOS of Zr_2N, but also the projected d states of a hypothetical ZrN structure within the Zr_2N structure (all N vacancies are filled in the so-called perfect structure). One can see that nitrogen vacancies give rise to additional states just below the Fermi level compared to its corresponding perfect structure, which originates from the Zr–Zr bonds passing through a nitrogen vacancy site. Such "vacancy states" usually lead to a drastic increase in the density of states at the Fermi level (0.076 in ZrN; 0.090 in Zr_6N_5; 0.112 in Zr_2N, states per eV per electron). The increasing density of the d state at the Fermi level can be interpreted as an increase in the $Zr(4d_\sigma)$–$Zr(4d_\sigma)$ bonding or metallic bonds between the zirconium atoms.

3.3 Mechanical properties

We further studied mechanical properties of the Zr–N compounds. The calculated elastic constants are shown in Table 1. All structures satisfy the Born–Huang stability criteria,[40] confirming their mechanical stability. From the calculated elastic constants, we can find ZrN holds the largest C_{11}, C_{22} and C_{33} values among the Zr_xN_y compounds, which indicate the very high compressibility along the axis directions. o-Zr_3N_4 has the smallest C_{11} and C_{44} values. The bulk modulus B, shear modulus G, Young's modulus E and Poisson's ratio ν were further obtained using the Voigt–Reuss–Hill averaging,[41] shown in Table 1. The calculated B values of zirconium nitrides are

Table 1 The calculated bulk modulus B, shear modulus G, Young's modulus E, Poisson's ratio ν, B/G ratio, anisotropy index A^U, Šimůnek's hardness H_S and Chen's hardness H_C of Zr_xN_y compounds at 0 GPa (B, G, E and H, GPa)

Phase	C_1	C_{12}	C_{13}	C_{15}	C_{22}	C_{23}	C_{25}	C_{33}	C_{35}	C_{44}	C_{46}	C_{55}	C_{66}	B	G	E	ν	B/G	A^U	H_S	H_C
Zr_2N	305	142	108					362		119			114	187	109	274	0.256	1.721	0.116	14.8	13.5
Zr_3N_2	293	132	130		325	93		384		112		96	84	190	100	255	0.276	1.896	0.170	15.5	11.0
Zr_4N_3	336	147	140	8	349	127	2	371	13	127	−10	95	109	209	108	277	0.280	1.931	0.091	15.2	11.3
Zr_6N_5	376	135	159	−25	384	153	29	364	2	118	25	134	145	224	122	309	0.270	1.845	0.233	15.3	13.2
Zr_8N_7	394	137	171	−28	396	162	31	385	2	131	35	154	147	235	129	328	0.267	1.815	0.301	13.3	14.1
ZrN^a	556	123								113				267	147	372	0.268	1.818	0.534	15.6	15.4
$Zr_{15}N_{16}$	437	153	155	−16	467	117	1	468	20	154	−13	130	161	247	148	369	0.251	1.673	0.323	15.5	17.3
Zr_7N_8	422	132	146	30	421	157	−30	396	2	150	28	166	160	234	146	362	0.242	1.605	0.199	15.5	18.2
Zr_4N_5	338	120	159	−11	425	116	−9	378	21	139	−12	106	118	215	120	303	0.264	1.789	0.211	15.0	13.7
o-$Zr_3N_4^b$	209	159	164		469	167		422		95		63	130	214	91	239	0.314	2.359	1.043	12.4	7.3
c-$Zr_3N_4^c$	423	146								133				238	135	341	0.261	1.761	0.002	11.0	15.2

^{a} $B = 249$,[34] $G = 157$,[35] $H_\nu = 16$.[36] ^{b} $B = 203$,[37] 238,[38] $H_\nu = 12.4$.[37] ^{c} $B = 224$,[37] $H_\nu = 11.7$,[39] 11.4.[37]
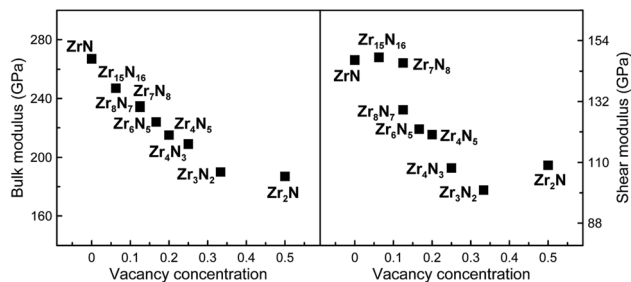
Fig. 4 Calculated bulk and shear moduli of the rocksalt structures as a function of vacancy concentration; also rutile-like Zr_2N is shown (its structure can also be represented as a close-packed metal sublattice with 1/2 octahedral voids occupied by nitrogen atoms).
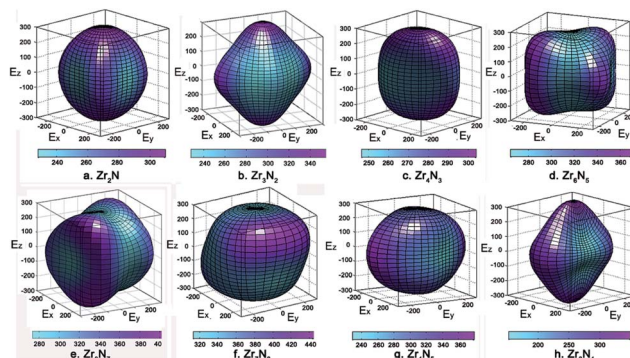

Fig. 5 Directional dependence of Young's moduli (in GPa) of the Zr_xN_y compounds.

comparable with many other transition metal carbides, nitrides and borides, such as Fe_3C (224 GPa (ref. 42)), TiN (294 GPa (ref. 31)) and TiB_2 (213 GPa (ref. 43)), but much lower than diamond (437 GPa (ref. 44)). Among these Zr_xN_y compounds, ZrN has the largest bulk and shear moduli, although Zr_7N_8 has a practically identical shear modulus (see Table 1).

The effect of vacancy concentration on bulk and shear moduli of the rocksalt Zr_xN_y structures is shown in Fig. 4. It can be seen that bulk and shear moduli monotonically decrease with increasing vacancy concentration. When N vacancies increase in a rocksalt structures, the number of Zr–N bonds obviously decreases. Moreover, the computed Zr–N separations are increasing when N vacancies increase, i.e. from 2.24 to 2.27 Å in Zr_8N_7 and Zr_2N, reflecting the weakening of the Zr–N bonding. Therefore, one may understand our findings, i.e. the loss of B and G is mainly attributed to the disappearance of some strong covalent Zr–N bonds.

For brittle materials, B/G ratio is smaller than 1.75 (ref. 45) (for example, for diamond $B/G = 0.8$). From Table 1, we can find that B/G values decreases in the following sequence: o-Zr_3N_4 > Zr_4N_3 > Zr_3N_2 > Zr_6N_5 > ZrN > Zr_8N_7 > Zr_4N_5 > c-Zr_3N_4 > Zr_2N > $Zr_{15}N_{16}$ > Zr_7N_8. B/G values of Zr_2N (1.721), $Zr_{15}N_{16}$ (1.673) and Zr_7N_8 (1.605) are smaller than 1.75, which indicate that these are brittle or borderline materials. For the other compounds, B/G values are larger than 1.75, which suggest that they are ductile materials. For ZrN, B/G value is slightly larger than 1.75, making a good compromise between hardness and ductility, which is mainly due to a peculiar interplay between metallicity and covalency. Besides, we can find that B/G values of Zr-rich phases are larger than N-rich ones except Zr_2N and o-Zr_3N_4. Obviously, the higher metal content, the more ductile the material. Surprisingly, semiconducting o-Zr_3N_4 has the largest B/G value (2.359) due to the low C_{11} and C_{44}, and o-Zr_3N_4 also possesses remarkable elastic anisotropy. Here, we used the Ranganathan and Ostoja-Starzewski method[46] to estimate anisotropy:

$$A^U = 5\frac{G^V}{G^R} + \frac{B^V}{B^R} - 6 \tag{2}$$

where G^V, B^V, G^R and B^R are the shear and bulk moduli estimated using the Voigt and Reuss methods, respectively.

The calculated anisotropy parameters A^U of Zr_xN_y phases are listed in Table 1. Elastic anisotropy decreases in the following

sequence: o-Zr_3N_4 > ZrN > $Zr_{15}N_{16}$ > Zr_8N_7 > Zr_6N_5 > Zr_4N_5 > Zr_7N_8 > Zr_3N_2 > Zr_2N > Zr_4N_3 > c-Zr_3N_4. Fig. 5 shows the directional dependence of Young's moduli for the selected Zr_xN_y compounds (see eqn (8) in ESI†). For an isotropic system, one would see a spherical shape. The degree of elastic anisotropy can be directly reflected from the degree of deviation in shape from a sphere. From Fig. 5, we can find that Young's modulus is more anisotropic in o-Zr_3N_4, while Zr_4N_3 and Zr_2N show more isotropic features. The anisotropy of o-Zr_3N_4 is due to low C_{11} and high C_{22}, C_{33} values, resulting in a flat shape of Young's modulus.

The Vickers hardness of zirconium nitrides was estimated by using Chen's model,[47] as follows:

$$H_C = 2(\kappa^2 G)^{0.585} - 3 \tag{3}$$

where κ is the Pugh ratio:[45] $\kappa = G/B$. The computed hardness values are given in Table 1. The estimated hardness of ZrN is 15.4 GPa, which is consistent with the experimental value of 16 GPa of Lévy et al.[36] Among these Zr_xN_y compounds, Zr_7N_8 has the highest hardness of 18.2 GPa. Given that Chen's model is based solely on the computed elastic constants, here we also used the Šimúnek method to estimate their hardness, which is mainly based on bond density and bond strength.[48] The corresponding expression is given as follows:

$$H_S = \frac{C}{\Omega} n \left[\prod_{i,j=1}^{n} b_{ij} s_{ij} \right]^{1/n} e^{-\sigma f_e} \tag{4}$$

where s_{ij} is the bond strength between atom i and j, b_{ij} is the bond number, Ω is the volume of the cell. The semi-empirical constants C and σ equal to 1450 and 2.8, respectively. The calculated hardness values are also given in Table 1. For the substoichiometric phases, the estimated hardness values are around 15 GPa. For Zr_3N_4, we found hardness values of 12.4 and 11.0 GPa for o-Zr_3N_4 and c-Zr_3N_4, respectively, which is consistent with previous theoretical calculations.[37,39] The reported Vickers hardness of c-Zr_3N_4 film is 36 GPa,[14,49] making it nearly a superhard film material. It is possible that hardness could be much higher in a thin film compared to a bulk crystal.[37] Certainly, more extensive hardness experiments for the Zr_xN_y structures should be performed.

4 Conclusions

By using the variable-composition *ab initio* evolutionary algorithm USPEX, we explored stable and metastable compounds in the Zr–N system at ambient pressure. Our calculations revealed that ZrN, Zr_2N, Zr_4N_3, Zr_6N_5, Zr_8N_7, $Zr_{15}N_{16}$, Zr_7N_8 and Zr_4N_5 are thermodynamically stable compounds at low temperatures, while Zr_3N_2 is marginally metastable and could be stable at high temperatures. Particularly, we found the two controversial compounds discovered by Juza *et al.* could be $Zr_{15}N_{16}$ and Zr_4N_5. The newly discovered compounds have defective rocksalt structures with ordered nitrogen or zirconium vacancies. The calculated elastic constants of zirconium nitrides are in good agreement with available experimental values. Our results show that bulk and shear moduli monotonically increase with decreasing vacancy content. This can be attributed to the occurrence of more Zr–N covalent bonds and weakening of the ductile Zr–Zr metallic bonds. Besides, we found hardness of bulk Zr_3N_4 is below $\sim$15 GPa.

Acknowledgements

References

1 H. O. Pierson, *Handbook of refractory carbides and nitrides: properties, characteristics, processing and applications*, Noyes Publication, New York, 1996, pp. 163–180.

2 H. Holleck, *J. Vac. Sci. Technol., A*, 1986, **4**, 2661–2669.

3 K. Inumaru, T. Ohara, K. Tanaka and S. Yamanaka, *Appl. Surf. Sci.*, 2004, **235**, 460–464.

4 D. J. Kim, Y. R. Cho, M. J. Lee, J. M. Hong, Y. K. Kim and K. H. Lee, *Surf. Coat. Technol.*, 1999, **116**, 906–910.

5 A. I. Gusev and A. A. Rempel, *Phys. Status Solidi A*, 1997, **163**, 273–304.

6 D. I. Bazhanov, A. A. Knizhnik, A. A. Safonov, A. A. Bagaturyants, M. W. Stoker and A. A. Korkin, *J. Appl. Phys.*, 2005, **97**, 044108.

7 R. Niewa and F. J. DiSalvo, *Chem. Mater.*, 1998, **10**, 2733–2752.

8 A. Kafizas, C. J. Carmalt and I. P. Parkin, *Coord. Chem. Rev.*, 2013, **257**, 207–2119.

9 A. Salamat, A. L. Hector, P. Kroll and P. F. McMillan, *Coord. Chem. Rev.*, 2013, **257**, 2063–2072.

10 S. V. Didziulis and K. D. Butcher, *Coord. Chem. Rev.*, 2013, **257**, 93–109.

11 L. Gribaudo, D. Arias and J. Abriata, *J. Phase Equilib.*, 1994, **15**, 441–449.

12 A. Zerr, G. Miehe and R. Riedel, *Nat. Mater.*, 2003, **2**, 185–189.

13 P. Kroll, *Phys. Rev. Lett.*, 2003, **90**, 125501.

14 M. Chhowalla and H. E. Unalan, *Nat. Mater.*, 2005, **4**, 317–322.

15 W. H. Baur and M. Lerch, *Z. Anorg. Allg. Chem.*, 1996, **622**, 1729–1730.

16 R. Juza, A. Gabel, H. Rabenau and W. Klose, *Z. Anorg. Allg. Chem.*, 1964, **329**, 136–145.

17 A. R. Oganov and C. W. Glass, *J. Chem. Phys.*, 2006, **124**, 244704.

18 A. R. Oganov, A. O. Lyakhov, M. Valle, C. Gatti and Y. Ma, *Rev. Mineral. Geochem.*, 2010, **71**, 271–298.

19 A. R. Oganov, A. O. Lyakhov and M. Valle, *Acc. Chem. Res.*, 2011, **44**, 227–237.

20 A. O. Lyakhov, A. R. Oganov, H. T. Stokes and Q. Zhu, *Comput. Phys. Commun.*, 2012, **184**, 1172–1182.

21 G. Kresse and J. Furthmller, *Phys. Rev. B: Condens. Matter*, 1996, **54**, 11169–11186.

22 J. P. Perdew, K. Burke and M. Ernzerhof, *Phys. Rev. Lett.*, 1996, **77**, 3865.

23 P. E. Blöchl, *Phys. Rev. B: Condens. Matter Mater. Phys.*, 1994, **50**, 17953.

24 M. Methfessel and A. T. Paxton, *Phys. Rev. B: Condens. Matter Mater. Phys.*, 1989, **40**, 3616–3621.

25 A. Togo, F. Oba and I. Tanaka, *Phys. Rev. B: Condens. Matter Mater. Phys.*, 2008, **78**, 134106.

26 H. Tang, A. Van der Ven and B. L. Trout, *Phys. Rev. B: Condens. Matter Mater. Phys.*, 2004, **70**, 045420.

27 M. Lerch, E. Füglein and J. Wrba, *Z. Anorg. Allg. Chem.*, 1996, **622**, 367–372.

28 Q. F. Zeng, J. H. Peng, A. R. Oganov, Q. Zhu, C. W. Xie, X. D. Zhang, D. Dong, L. T. Zhang and L. F. Cheng, *Phys. Rev. B: Condens. Matter Mater. Phys.*, 2013, **88**, 4269–4275.

29 X. X. Yu, C. R. Weinberger and G. B. Thompson, *Comput. Mater. Sci.*, 2016, **112**, 318–326.

30 C. Jiang and W. S. Jiang, *Phys. Status Solidi B*, 2014, **251**, 533–536.

31 S. Y. Yu, Q. F. Zeng, A. R. Oganov, G. Frapper and L. T. Zhang, *Phys. Chem. Chem. Phys.*, 2014, **17**, 11763–11769.

32 J. E. Huheey, *Inorganic chemistry: principles of structure and reactivity*, Harpar & Row, 1993, vol. 156, pp. 907–914.

33 R. Hoffmann, *Solids and surfaces: a chemist's view of bonding in extended structures*, Wiley-VCH, New York, 1988, pp. 18–21.

34 Z. Q. Chen, J. Wang and C. M. Li, *J. Alloys Compd.*, 2013, **575**, 137–144.

35 C. Sarioglu, *Surf. Coat. Technol.*, 2006, **201**, 707–717.

36 F. Lévy, P. Hones, P. Schmid, R. Sanjinés, M. Diserens and C. Wiemer, *Surf. Coat. Technol.*, 1999, **120**, 284–290.

37 F. M. Gao, *Chin. Phys. Lett.*, 2011, **28**, 076102.

38 W. Y. Ching, Y. N. Xu and L. Z. Ouyang, *Phys. Rev. B: Condens. Matter Mater. Phys.*, 2002, **66**, 126–130.

39 F. M. Gao, R. Xu and K. Liu, *Phys. Rev. B: Condens. Matter Mater. Phys.*, 2005, **71**, 2103.

40 F. Mouhat and F. X. Coudert, *Phys. Rev. B: Condens. Matter Mater. Phys.*, 2014, **90**, 224104.

41 W. Zhou, L. J. Liu, B. L. Li, P. Wu and Q. G. Song, *Comput. Mater. Sci.*, 2009, **46**, 921–931.

42 C. Jiang, S. G. Srinivasan, A. Caro and S. A. Maloy, *J. Appl. Phys.*, 2007, **103**, 3654–3660.

43 V. Milman and M. Warren, *J. Phys.: Condens. Matter*, 2001, **13**, 5585.

44 Y. C. Liang, W. L. Guo and Z. Fang, *Acta Phys. Sin.*, 2007, **56**, 4847–4855.

45 S. F. Pugh, *Philos. Mag.*, 1954, **45**, 823–843.

46 S. I. Ranganathan and M. Ostoja-Starzewski, *Phys. Rev. Lett.*, 2008, **101**, 055504.

47 X. Q. Chen, H. Y. Niu, D. Z. Li and Y. Y. Li, *Intermetallics*, 2011, **19**, 1275–1281.

48 A. Šimúnek, *Phys. Rev. B: Condens. Matter Mater. Phys.*, 2007, **75**, 172108.

49 A. Zerr, G. Miehe and R. Riedel, *Nat. Mater.*, 2003, **2**, 185–189.